

We are IntechOpen, the world's leading publisher of Open Access books Built by scientists, for scientists

6,900

Open access books available

186,000

International authors and editors

200M

Downloads

Our authors are among the

154

Countries delivered to

TOP 1%

most cited scientists

12.2%

Contributors from top 500 universities



WEB OF SCIENCE™

Selection of our books indexed in the Book Citation Index
in Web of Science™ Core Collection (BKCI)

Interested in publishing with us?
Contact book.department@intechopen.com

Numbers displayed above are based on latest data collected.
For more information visit www.intechopen.com



Porous Ceramic Sensors: Hydrocarbon Gas Leaks Detection

Yibrán A. Perera-Mercado,
Griselda Castruita-de León and
Geanette Polanco Piñerez

Additional information is available at the end of the chapter

<http://dx.doi.org/10.5772/intechopen.72315>

Abstract

According to the American National Standards Institute (ANSI), a sensor is a device which provides a usable output in response to a specified measurement of a physical quantity converted into a signal suitable for processing (e.g., optical, electrical, or mechanical signals). On the other hand, porous ceramic materials play an important role as sensor materials, because by selecting a suitable base ceramic material for the intended use and then adjusting their overall porosity, pore size distribution, and pore shape, they can cover different applications such as liquid-gas filters, insulators, catalytic supports, mixed of gases separators and sensors, among others. In addition, they have controlled permeability, high melting point, high superficial area, high corrosion and wear resistance, low expansion coefficient, tailored electronic properties, etc. Currently, a few niche areas demand sensors for compact electronic device design, e.g., leak inspections for oil and gas dispositive, flammable and/or toxic gas detection in waste storage areas and confined spaces, hydrocarbons and their associated gas detection at low temperatures and high humidity conditions, among others. In this chapter, the advances in porous ceramic production for hydrocarbons and associated gas detection will be presented and discussed.

Keywords: porous ceramic materials, sensors, hydrocarbons, mesoporosity, microporosity, macroporosity, nanomaterials, hydrocarbon leaks

1. Introduction

Sensors are key elements in the rapidly evolving fields of instrumentations, measurements, and automated systems. Different functions and materials have been investigated, and several devices have been put on the market or have become part of sophisticated instrumentations.

Among these materials, porous ceramics have played an important role because of their intrinsic physicochemical properties. They have also been widely used to satisfy diverse needs for sensing devices, and consistent results have been obtained in the field of atmospheric sensors, i.e., temperature, humidity, and presence of hydrocarbon gases sensors. In addition, the management of risk in oil and gas industrial installations is a priority task, especially when exploration and exploitation activities of the petroleum and gas sector in remote places and fragile environments are increasing rapidly. In particular, due to the nature of the working fluids in the oil industry, the risks associated to plant operations are considered as a high-risk activity. The risk management activity begins at the study and understanding of the hazards involved in a particular industrial activity, in order to establish security zones and secure procedures to be followed.

On the other hand, the current tendency of porous ceramic materials used in hydrocarbon leaks detection is shown in **Figure 1a**. The technological advances in this field indicate that 31% of these materials are based on tin oxide (SnO_2), followed by indium oxide (In_2O_3) with 23% and by zinc oxide (ZnO) that represents the 18%. These three metal oxides are the most common porous ceramic materials that have been using for sensing hydrocarbon and/or associated gases such as liquefied petroleum gas (LPG), methane, H_2 , NO_2 , ethanol, methanol, acetone, H_2S , CO , toluene, among others. However, several researchers have been testing additional oxides such as chromium oxide (Cr_2O_3), cobaltic oxide (Co_3O_4) tungsten trioxide (WO_3), and silicon dioxide (SiO_2) as potential porous ceramics with sensing properties. In addition, diverse elements are adding to the ceramic porous materials in order to improve their sensing capabilities. **Figure 1b** shows that palladium (Pd) with 32% is the most used element for doping the porous ceramic sensors for hydrocarbon leaks detection, followed by platinum (Pt), and vanadium (V) with 16%. Other elements such as cerium (Ce), gold (Au), tungsten (W), etc., were also identified as important secondary compounds of these kinds of sensing materials. These statistic data were generated based on the state-of-the-art developed for this specific book chapter and will be explained extensively in the following sections.

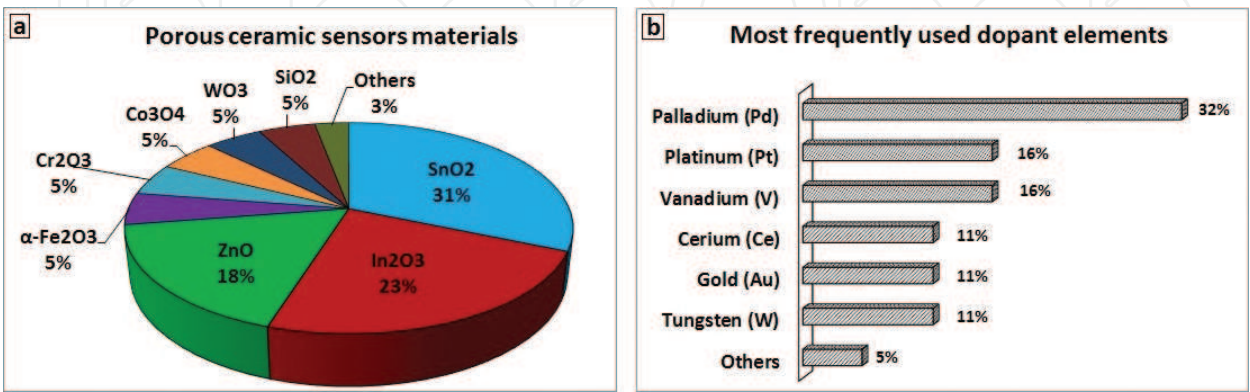


Figure 1. (a) Percentage distribution of the most used porous ceramic materials for sensing hydrocarbons and (b) percentage of elements most used for doping the porous ceramic sensor materials.

Therefore, the present chapter focuses on a complete review on the application of porous ceramic materials, as an important part of the new materials' generation, to detect leakages of hydrocarbons and their associated gases.

2. Porous ceramic materials: synthesis methods and characterization

A porous material is identified by the presence of channels, holes, or interstices. Ceramic materials with either ordered or disordered porosity in different size ranges have attracted the attention as sensing materials in the fields of hydrocarbon leaks detection and other important gases such as CO, CO₂, H₂, NH₃, NO_x, SO_x, and H₂S. Typical classification of porous materials is given by IUPAC depending on the pore size as follows: micropores (less than 2 nm), mesopores (2–50 nm), and macropores (more than 50 nm). The application and performance of porous materials in such fields lies in their physical, morphological, and textural properties. For example, high-specific surface area is of great importance, especially to interact with gases. Pore properties, such as pore size, porosity, and pore shape, also strongly influence on the desired performance of the material. Through different synthesis methods, the formation of porous ceramic materials is possible. Typical methods that are widely practiced are sol-gel synthesis, wet synthesis, impregnation, co-precipitation, and hydrothermal synthesis. Hydrothermal synthesis is the most common method to obtain a variety of nanostructured materials with different shapes, such as spheres, rods, wires, sheets, tubes, and so on. Others are sponge method, foam method, leaching, sintering of particles, emulsion templating, gel casting, and injection molding. More sophisticated methods have been developed to produce complex ceramic materials, for example, solution-combustion method. Many kinds of materials have received attention regarding gas sensors field. In the following text, a description of some relevant porous materials, their synthesis methods, and main characterization that determine their potential application in hydrocarbon and gas sensors is presented.

Zeolites are versatile materials that have found industrial applications in several fields such as water purification, catalysis, adsorption, and more recently in sensors for different hydrocarbons and gases [1–3]. Synthetic zeolites by hydrothermal method are obtained from Si and Al sources dissolved in water into an autoclave. Here, the growth of crystals is developed under high pressure and temperature in a closed system by controlling reaction temperature and time, precursors, and chemical composition of reaction mixture [4]. Novel strategy to synthesize nanozeolite LTA (Linde Type A) in its sodium form by hydrothermal method was reported by Anbia et al. [5]. In this report, pore size of 6–7 nm and BET surface areas around 500 m²/g were calculated by N₂ adsorption-desorption analysis. Novel approach of *in-situ* hydrothermal synthesis was applied to glass fibers coated with zeolite layer for chemical sensors toward ethane and propane [6]. SEM images showed homogeneous layer of zeolite crystals and XRD patterns confirmed the zeolite type structure.

ZnO has been successfully loaded into mesoporous ZSM-5 zeolites by simple wet impregnation method, which consists on the immersion of sample in solution of the corresponding metal oxide at determined concentration, temperature, and stirring [7]. In this way, sensors based on

ZnO particles have been fabricated toward CO, H₂, and H₂S, showing high preference to ethanol detection [8]. Additionally, zeolite has been used as layer support and overlay onto metal oxides as filters for modified gas sensors. In this regard, the sorption and catalytic properties of zeolites can improve the response of sensor and make it sensitive or insensitive to specific species. Layers of different porous zeolites such as silicalite, zeolite A, ZSM-5, LTA onto metal oxides (SnO₂, WO₃, and Cr₂O₃) have been assessed [9–12]. Seeding process and screen printing deposition seem to be common methodologies for fabrication of zeolite films onto metal oxides. The results of this investigation indicated an excellent discriminatory behavior when zeolite overlays were used, making the sensor more selective to specific gases even humidity or mixture-gas environments were tested. Nevertheless, in all cases, the sensor sensitivity was very dependent on the zeolite structure.

The combination of zeolite and conductive polymers has resulted in gas sensors lighter and less expensive with favorable operation on extreme conditions in comparison with metal sensors. Polythiophene (PT), polypyrrole (PPr), polyphenylene (PP), polyphenylenevinylene (PPV), and mainly polyaniline (PANI) have been taken into account for these purposes [13]. PANI/clinoptilolite and PT/zeolite 13X composites for CO sensors have been included by chemical oxidative polymerization of the respective monomer solution in presence of zeolite dispersion to promote the polymer penetration into zeolite pores [14]. The electrical conductivity sensitivity to CO increased significantly when zeolite content increased too, suggesting the higher amount of zeolite pores and surface area, the better interaction with gas molecules.

Since the discovery in 1990, mesoporous silica has had wide and varied field of application in catalysis, sorption, drug delivery, oil and gas industry, sensor fabrication, and so forth. Ordered mesoporous silica molecular sieves are produced widely by sol-gel method and also under hydrothermal conditions using a surfactant (cationic, anionic, or non-ionic) as template and either tetraethyl orthosilicate (TEOS) or sodium silicate as silica source [15, 16]. The first stage of sol-gel process involves the formation of colloidal suspension (sol) and then the gelation of the sol to form a network. Particularly, the synthesis of silica comprising the hydrolysis and condensation of silica source at specific pH conditions (acidic or basic pH) as catalyst of the reaction to form silica particles that precipitate after a nucleation and growth process [17]. The regulation of reaction conditions has been decisive in order to obtain well-ordered pore structure with defined morphology. During synthesis processes, time and temperature aging, pH of solution, type of surfactant, and co-surfactant have been evaluated to investigate the effect of reaction conditions on the structural and textural properties of silica particles [18]. Micelles

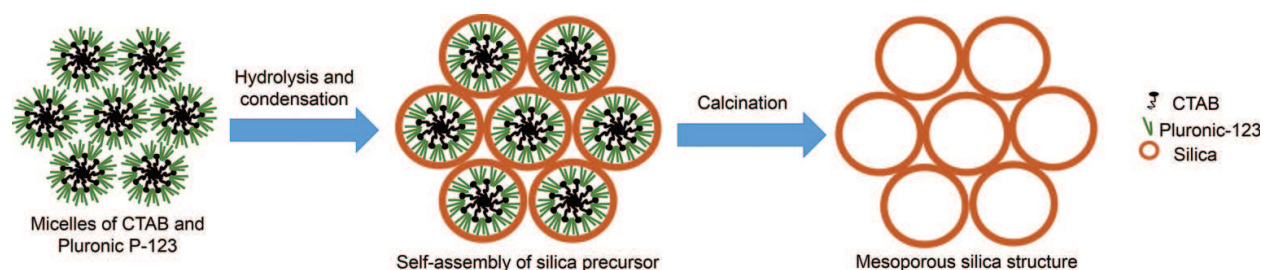


Figure 2. Proposed mechanism for synthesis of spherical SBA-15.

formed by Pluronic 123 and cetyltrimethylammonium bromide (CTAB) as template and co-template, respectively, induced the co-assembling of hydrolyzed silicate species from TEOS to synthesize spherical SBA-15 mesoporous silica with potential application in gas adsorption processes (**Figure 2**) [19]. Silica particles were not obtained when Pluronic 123/CTAB molar ratio was less than 0.31. After synthesis, samples were calcined for surfactant and co-surfactant elimination. Samples calcined at 540°C showed narrow pore size distribution with an average pore size of 3 nm and BET surface area of 667 m²/g. The analysis of thermally treated samples at 850°C indicated the structural order and spherical morphology were maintained.

Mesoporous MCM-41 silica was synthesized by hydrothermal method at several pH values [20]. Well-ordered hexagonal mesoporous structure was validated by TEM (transmission electron microscopy) images and XRD patterns which showed the characteristic reflection peaks indexed to the planes [100, 110, 200] of this type of silica. Yang et al. [21] synthesized hierarchical porous wheat-like silica particles by sol-gel method and co-hydrothermal aging. Bimodal mesoporous structure (average pore size of 2–10 nm) determined by N₂ adsorption-desorption measurements was achieved through controlling the templates ratio and pH solution. Microwave-assisted hydrothermal methodology has allowed the preparation of mesoporous silica particles in shorter reaction time with similar structural and textural properties to those obtained by conventional hydrothermal route [22].

On the other hand, sol-gel method has been also applied for silica synthesis with no hydrothermal conditions. Spherical mesoporous MCM-48 silica have been successfully obtained at room temperature conditions from TEOS [23]. High structural ordering of mesoporous evidenced by XRD patterns and TEM images was achieved by varying the reaction time, surfactant/TEOS, and water/ethanol ratios. Uniform spherical MCM-48 silica particles with high surface area (900–1800 m²/g) and average pore diameter of 2 nm were obtained by modulating reaction conditions and initial gel composition [24]. SEM and HR-TEM images of *in-situ* amino-functionalized MCM-48 mesoporous silica are shown in **Figure 3**. Spherical particles with well-ordered pore structure were achieved at 7 h of reaction time with particle size between 200 and 500 nm [25].

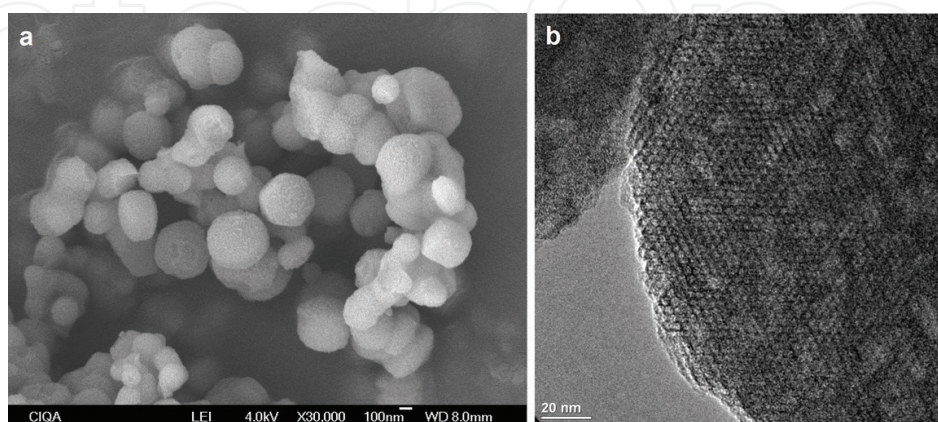


Figure 3. SEM (a) and HR-TEM (b) images of *in-situ* amino-functionalized mesoporous MCM-48 silica synthesized by sol-gel at room temperature.

Due of the high-specific surface area and low density, silica aerogels prepared by sol-gel method have received attention for gas sensing purposes [26]. Nanofibers embedded in hydrophobic silica aerogel synthesized from a sol comprising tetramethyl orthosilicate, methanol, and water in basic medium were investigated by Xiao et al. for acetylene detection [27]. SEM images showed the nanofibers 200 nm long and 0.8 μm diameter well-embedded in the aerogel. The porosity of aerogel allowed the fiber performance as evanescent-field gas sensor. Silica can be used as template or coating for other components such as metal oxides. ZnO nanoparticles coated with mesoporous silica through a simple sol-gel method were reported by El-Nahhal et al. [28]. The change on the displacement of XRD peaks and the elemental analysis by EDX (energy-dispersive X-ray spectroscopy) confirmed the presence of silica. Additional evidence through TEM images was provided, where a worm-like silica structure coated the dark ZnO nanoparticles. Li et al. [29] reported the use of SBA-15 (Santa Barbara Amorphous-15) silica as template for mesoporous NiO nanowires to be assessed as sensor toward ethanol. In this work, SBA-15 silica was prepared by hydrothermal method, after that, NiO nanowires was synthesized by nanocasting method which consisted on the dissolution and dispersion of the NiO precursor ($\text{Ni}(\text{NO}_3)_2$) and the silica particles under stirring and heating. After, the resulting powder was calcined and SBA-15 silica was removed with NaOH aqueous solution. Mesoporous NiO nanowires with high surface area (111 m^2/g) and average pore size of 3.6 nm were achieved. These characteristics make them more sensitive to ethanol gas in the range of 50–3000 ppm.

Porous alumina (Al_2O_3) is other kind of material that has had an important role as ceramic support of metal oxides for gas sensors due to its insulating properties and inert chemical behavior [30]. A conventional method used to prepare it is by means of solid-phase transformation through thermal decomposition of aluminum hydroxides. Alumina precursors can be synthesized by sol-gel process where an aluminum salt, such as AlCl_3 , AlNO_3 , $\text{Al}_2(\text{SO}_4)_3$, is hydrolyzed to form the corresponding aluminum hydroxide which precipitates [31]. The thermal treatment at different temperatures leads several transition alumina and α -alumina with highly porous vermicular microstructure as can be appreciated in **Figure 4**.

On the other hand, γ -alumina loaded at 20 wt% with various metal oxides (CeO_2 , CuO , Fe_2O_3 , Mn_2O_3 , NiO , and RuO_2) were prepared by Hyodo et al. [32] for VOC sensing. The mesoporous γ -alumina was synthesized by microwave-assisted solvothermal method from hydrolysis of

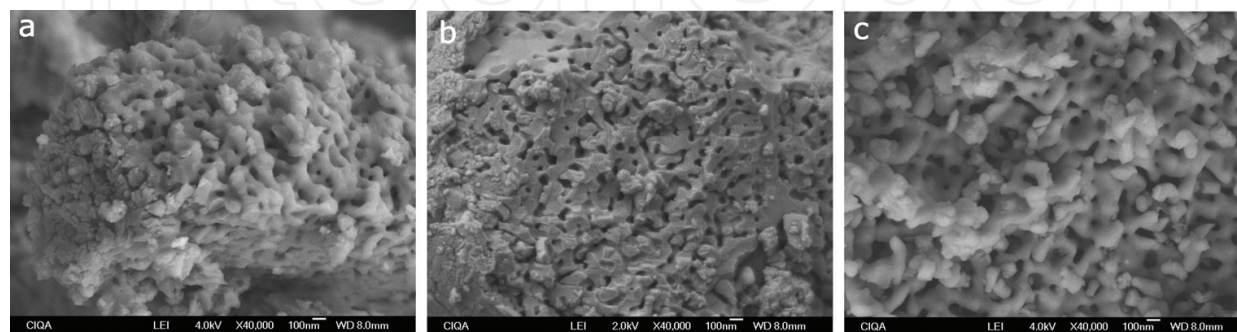


Figure 4. SEM images of α -alumina synthesized by sol-gel method from different aluminum salts. (a) Precursor of AlNO_3 ; (b) precursor of AlCl_3 ; (c) precursor of $\text{Al}_2(\text{SO}_4)_3$.

aluminum butoxide in propanol/water solution under heating to form a white precipitate. The precipitate was impregnated with the solution of the corresponding metal oxide precursor and the mixture was treated by firing at 700°C to obtain the loaded γ -alumina powder. The metal oxide-alumina powders showed high specific surface areas (around 200 m²/g) and were able to detect ethanol, and other VOC such as acetone, ethyl acetate, benzene, toluene, and o-xylene. Porous alumina synthesized via anodic oxidation of aluminum, denoted as porous anodic alumina, has been object of numerous studies as template on which metal oxides are deposited for the development of gas sensor systems. The anodizing process consists of exposure the aluminum specimens to certain voltage conditions in an electrolyte solution. Anodization conditions, such as type of electrolyte, anodizing potential, temperature, and duration of process, determine the morphology and microstructure of porous film. Sharma and Islam [33] found that the increasing voltage caused an increase of pore size due to greater dissolution of the oxide layer. Likewise, the porous structure of alumina provided the nucleation sites for uniform growth of Pd-capped Mg when was deposited on it, and a finer film was obtained as was appreciated in XRD patterns and SEM images. Norek et al. [34] argued that the pores of alumina provided enough space for free expansion of metallic film, avoiding the accumulation of stress and resulting in a greater H₂ absorption capacity. In the same way, active layers of WO₃ and NbO₂ were deposited onto anodic porous alumina by sputter-deposition [35]. The critical combination of the high quality and reproducible porous structure of alumina film significantly influenced the sensor response to H₂ in a range of 5–1000 ppm and operating temperatures of 20–350°C.

3. Porous ceramic materials for sensors. Operational principles for gases detection

The complex operational mechanism of porous ceramic sensors for hydrocarbon gases is affected by factors, such as chemical composition, humidity, temperature, morphology, and so on. This mechanism is determined by chemical and electronic interactions between the porous ceramic and the specific gas resulting in a resistance change. The main operational principles of sensing devices are shown in **Table 1** [36].

There are three principal reasons for monitoring hydrocarbon gases: (1) combustible/flammable gas, (2) toxic/irritant gases and (3) oxygen levels control. As is well known, any hydrocarbon leaks is a potential explosive hazard, where to avoid an explosion, atmospheric levels must be maintained below the lower explosive limit (LEL) for each gas, or purged of oxygen. In addition, for a flame to exist, three conditions must be met: (1) a source of fuel (any hydrocarbon source, e.g., methane or gasoline vapors), (2) enough oxygen (greater than 10–15%) to oxidize or burn the fuel, and (3) a source of heat (ignition) to start the process [36]. Moreover, combustion can occur at both extreme low-end and high-end gas concentrations. These extremes are called the lower explosive limit (LEL) also known as lower flammability limit (LFL), and the upper explosive limit (UEL) or upper flammability limit (UFL). Any gas or vapor concentration that falls between these two limits is in the flammable (explosive) range [36]. Therefore, the control and knowledge about the sensors' operational conditions

Gas detection technology	Operational description	Gas type detected
Catalytic bead	A wire coil is coated with a catalyst-coated glass or ceramic material, and is electrically heated to a temperature that allows it to burn (catalyze) the gas being monitored, releasing heat, and increasing the temperature of the wire. As the temperature of the wire increases, so does its electrical resistance. This resistance is measured by a Wheatstone Bridge circuit and the resulting measurement is converted to an electrical signal used by gas detectors. A second sensor, the compensator, is used to compensate for temperature, pressure and humidity	Combustible gas
Metal oxide semiconductor (also known as "solid state")	A semiconducting material (metal oxide) is applied to a non-conducting substrate between two electrodes. The substrate is heated to a temperature at which the presence of the gas can cause a reversible change in the conductivity of the semi-conducting material. When no gas is present, oxygen is ionized onto the surface and the sensor becomes semi-conductive; when molecules of the gas of interest are present, they replace the oxygen ions, decreasing the resistance between the electrodes. This change is measured electrically and is proportional to the concentration of the gas being measured	Combustible gas; toxic gas
Point infrared (IR) short path	Uses an electrically modulated source of IR energy and two detectors that convert the IR energy into electrical signals. Each detector is sensitive to a different range of wavelengths in the IR portion of the spectrum. The source emission is directed through a window in the main enclosure into an open volume. A mirror may be used at the end of this volume to direct the energy back through the window and onto the detectors. The presence of a combustible gas will reduce the intensity of the source emission reaching the analytical detector, but not the intensity of emission reaching the reference detector. The microprocessor monitors the ratio of these two signals and correlates this to a %LEL reading	Combustible gas
Open (long path) infrared	Open-path IR monitors expand the concepts of point IR detection to a gas sampling path of up to 100 m. Like point IR monitors, they utilize a dual beam concept. The "sample" beam is in the infrared wavelength which absorbs hydrocarbons, while the second "reference" beam is outside this gas absorbing wavelength. The ratio of the two beams is continuously compared. When no gas is present, the signal ratio is constant; when a gas cloud crosses the beam, the sample signal is absorbed or reduced in proportion to the amount of gas present while the reference beam is not. System calculates the product of the average gas concentration and the gas cloud width, and readings are given in %LEL/meter.	Combustible gas
Photoacoustic infrared	The gas sample is exposed to infrared light; as it absorbs light, its molecules generate a pressure pulse. The magnitude of the pressure pulse indicates the gas concentration present	Combustible gas; toxic gas
Electrochemical for toxic gas or/and oxygen detection	Sensor is a chamber containing a gel or electrolyte and two active electrodes—the measuring (sensing/working) electrode (anode) and the counter electrode (cathode). A third electrode (reference) is used to build up a constant voltage between the anode and the cathode. The gas sample enters the casing through a membrane; oxidation occurs at the anode and reduction takes place at the cathode. When the positive ions flow to the cathode and the negative ions flow to the anode, a current proportional to the gas concentration is generated	Toxic gas or oxygen deficiency/enrichment

Gas detection technology	Operational description	Gas type detected
Thermal conductivity	Two sensors (detecting and compensating sensors) are built into a Wheatstone Bridge. The detecting sensor is exposed to the gas of interest; the compensating sensor is enclosed in a sealed compartment filled with clean air. Exposure to the gas sample causes the detecting sensor to cool, changing the electrical resistance. This change is proportional to the gas concentration. The compensating sensor is used to verify that the temperature change is caused by the gas of interest and not by other factors	Combustible gas; toxic gases
Photoionization	A photoionization detector (PID) uses an ultraviolet lamp to ionize the compound of interest. Ions are collected on a "getter," a current is produced and the concentration of the compound is displayed in parts per million on the instrument meter	Toxic (organic compounds)

Table 1. Types of gas detection technologies and their operational descriptions [36].

are the master key to understand the hydrocarbon gases monitoring process in order to get alarms before a potential explosive condition occurs. On the other hand, the developments of low cost and power efficient devices that can selectively detect hazardous analytes with very high sensitivity have evolved constantly. Two main operating principles have been intensely investigated: catalytic sensors and metal oxide semiconductor (MOS) have been investigated in sensors for wide range of chemical analytes [37].

Catalytic sensors are very common to detect combustible gases. These consist of two elements: a detector element which contains the sensitive material and an inert compensator element. The operating principle is based on the oxidation reaction of the combustible gas with the detector element. The heat released by this exothermic reaction changes the electrical resistance of the detector element. Combustible gas does not burn on the compensator element, so its temperature and resistance are maintained unchanged. When sensor is located at combustible gas-free atmosphere, a balance of the bridge circuit is maintained. On the contrary, when combustible gases are present, the resistance of the detector element increases and causes an imbalance in the bridge circuit producing an output voltage signal, which is proportional to the combustible gas concentration. This kind of sensors is very sensitive to environmental conditions such as temperature, humidity, and pressure. On the other hand, basic electrochemical-type sensors consist on a working electrode, a counter electrode, and an ion conductor. An electrical signal is produced by the chemical reaction (oxidation or reduction) of the analyte (gas) with the working electrode, giving a current proportional to the gas concentration that flows between electrodes [38]. This kind of sensor depends on establishment of an electrochemical potential which is not affected by surface morphology. Electrochemical sensors are minimally affected by pressure, but they are very sensitive to temperature.

In MOS sensors, a metal oxide is used as sensing material. In a typical MOS sensor, oxygen is adsorbed onto the surface of the sensing material (i.e., SnO_2 , ZnO , In_2O_3 , TiO_2 , and WO_3). These oxygen molecules attract free electrons from the metal oxide which forming a potential barrier to prevent electron flow. If sensor is exposed to certain gas atmosphere, the gas reacts with the

oxygen molecules through a reducing reaction which causes the release of electrons and allows that a current flows freely through the sensor. Consequently, the gas concentration is detected by the resistance change of MOS [4]. This kind of sensor seems to be the most important because the huge amount of investigation regarding to them. Pt nanoparticles-modified Al-doped ZnO (AZO) porous macro/mesoporous nanosheets prepared by solution combustion method were assessed for butane gas sensor at low temperature. The large surface area of 50.17 m²/g and the broad pore size distribution between 3 and 110 nm calculated by BJH method provided a good contacting interface between sensing material and gas molecules allowing a maximum response of 56–3000 ppm of butane. The gas sensitivity is related to the electron flow through the interface from AZO to Pt. An oxidation-reduction reaction happened when Pt nanoparticles-modified AZO nanosheets were exposed to reducing gas. A large amount of electrons are released which back to the conduction band of AZO leading a decrease of resistance [39]. Hierarchical flower-like structure composite formed by combination of metal oxides with high surface area and porous structure have shown improved gas sensing performance in comparison with pure metal oxide. NiO:CuO nanocomposites (molar ratio 1:1) showed 2 s response time to 100 ppm NO₂ at room temperature and relative humidity of 42%. The heterojunction formed at the interface between NiO and CuO could accelerate the speed response. O₂ molecules are absorbed on the surface of sensor when it is exposed to air. These O₂ molecules capture electrons from conduction band of sensing material forming ions O₂⁻. At NO₂ atmosphere, these gas molecules are adsorbed onto the surface by extracting electron from conduction band. Because electrons are transferred to NO₂, the resistance is decreased [40].

The combination of p-type Sb₂O₅ with n-type SnO₂ in composite sensor for NO₂ have also evaluated thought output voltage measurements and the sensing response was defined by the ratio of sensor resistance in NO₂ and air atmospheres. Relevant results indicate low operation temperature (100°C) and high response (800–5 ppm NO₂) at short time (5 s) of composite sensor. The existence of p-n junction in composite sensor which induced a new potential barrier when electrons transfer between SnO₂ particles, large surface area and porous structure of Sb₂O₅ and SnO₂ particles gave benefits to exhibit superior gas sensing performance. The reduction of operating temperature was attributed to lower energy required for electron transition derived from the decrease of band gap of p- and n-type semiconductor [41]. In another work, porous hollow balls formed by self-assembly of α-Fe₂O₃ nanoparticles were synthesized by hydrothermal method and were evaluated for sensing ethanol, CO, and NH₃ in a temperature range from 250 to 450°C. Sensor response (S) was determined following the equation $S = R_{\text{air}}/R_{\text{gas}}$, where R_{air} and R_{gas} are the sensor resistances recorded in presence of test gas and dry air, respectively. The initial resistance of α-Fe₂O₃ hollow balls sensor decreasing when operating temperature increasing, leading 85 kΩ at 250°C and 18 kΩ at 450°C in ethanol sensing test. In addition, the sensor response increased from 1.77 to 3.29 with increasing ethanol concentration from 50 to 500 ppm at 400°C. Low sensor response to CO and NH₃ was detected, thus, this sensor is suggested only for ethanol detection [42]. In order to improve its ethanol sensing capability at the temperature range between 25 until 125°C, other researchers have been introduced Au nanoparticles into ZnO nanostructures by sputtering technique. The sensing mechanism is based on the surface electron density changes of the semiconductor. The oxygen molecules in air react to the surface electrons of ZnO forming oxygen species determined by the constant reaction k_{oxy} as follows:

$O_2 (ads) + e^- (surface) \leftrightarrow O_2 (ads)$ [43]. The Au nanoparticles act as the catalyst leading oxygen dissociation. In this way, the k_{oxy} in chemical reaction allows an improved sensor response. The resistance values showed a reduction when sensor was exposed to ethanol vapor. If the ethanol exposition is stopped, the sensor resistance returned to the initial state. Moreover, the resistance response is improved when UV illumination is included in tests. This behavior is associated to the large density of active photoelectrons due to the UV excitation [10]. Novel approaches toward ethanol sensor enhancement using decorated metal oxides have recently studied [44]. Improved ethanol sensing at operating temperature of 160°C and response of 70.2–100 ppm was reported by using porous SnO_2 nanosheets loaded with Au nanoparticles, which means a response three times higher than those obtained with SnO_2 -based sensor. The response curves increased with increasing ethanol concentration and returned to baseline when ethanol supply was stopped inside test chamber, indicating quick response and recovery time. The synergistic effect of 2D porous structure of SnO_2 which allowed facile gas diffusion and the catalytic activity of Ag particles allowed superior ethanol-detection properties [45]. The fabrication of NiO/ZnO nanoplates by solvothermal method and thermal treatment is also reported. The ratio of the electrical resistance in air R_a , and electrical resistance in ethanol-air mixed gas was used to determine the sensor performance. The response to ethanol in NiO/ZnO sensor is better than those in NiO gas sensor. A short response of 2.1 s and time recovery of 4 s promised good sensor performance for ethanol sensing [8]. Colloidal ZnO quantum dots treated with $ZnCl_2$ and annealing at 200–300°C were used to fabricate gas sensor toward H_2S . Nearly, no response (1.07–50 ppm H_2S) was obtained with untreated ZnO sensor whereas $ZnCl_2$ -treatment ZnO sensor showed a response up to 5 with very slow recovery. Recovery properties were improved by annealing at 300°C for 1 h. Sensor under that conditions at room temperature reached a response of 113.5 and recovery time of 820 s. Based on results, the fast and sensitive response makes this sensor very attractive in comparison with others [46]. Changes in resistance of porous $BiNbO_4$ nanostructures-based sensors were reported for selective NH_3 sensing. The complete oxidization of NH_3 onto the sensor surface makes changes on the conductivity sensor. The maximum response of 16 s and recovery time less than 17 s were attributed to the large surface area (41.27 m^2/g) and high porosity that increase the accessible sites for adsorption of gas molecules [47].

4. Specific application: hydrocarbon leak sensors. The thermomechanics principles

Diverse fluids used in the petrochemicals processes such as propane, liquid petroleum gas (LPG), butane, propylene; and other organics and inorganics fluids are widely stored, transported, or used in a pressure-liquefied state. Therefore, these fluids are very important in the industry when leak sensing technology is needed. Specifically, pressure-liquefied gas (PLG) have a high probability of ending in a fatal accidental leak due to its own fluid properties and behavior [48, 49]. So, sensing technology needed must cover a range of fluids; however, there are some clear examples where the widely and frequently used of some fluids highlight some extra needs for specially design sensors or sensing technology.

4.1. Theoretical basis of the problem: phenomenon involved

Flashing depends on the initial parameter values of the fluid as pressure and temperature as well as the type of fluid. A particular combination of those variables can create, for some cases, a complete breaking of the liquid core into droplets at the same time that it is going out of container like unstable two phase jet or liquid jet. The major difficulty in the understanding of this flashing phenomenon and the parameters interactions within it belongs to the existence of a compromise between the physical and thermodynamics mechanism that acts on the released fluid [50]. Specific behavior and characteristics of these liquid-gas mixtures and the potential for the formation of vapor-liquid aerosols during a superheated liquid release due to the breaking of the metastable state can significantly affect the hazard zone and the mitigation steps that can be taken to minimize the release impact for the hydrocarbon industry [49, 51, 52].

High complexity level of the whole process in combination with the need of more information based on experimental, analytical, or numerical models is the main difficulty to be overcome in order to develop new sensing technology. Different authors have concentrated efforts on the jet characterization. The developed information about the jet can help to understand the parameters that can be used as key indicators of accidental release of hydrocarbons.

Flashing phenomenon complexity required calculation of the velocity discharge, void fraction, and mass flow of a flashing jet together with the estimation of the temperature. Due to the nature of the nucleation process, the assumptions of adiabatic flow with non-reversible work for the surface tension forces are made. Those considerations are found to be more realistic than the isentropic condition used until now by different authors. Dynamics conditions usually considered include the mixture velocity after flashing as critical conditions. Frequently numerical modeling techniques are only applied after the flashing jet is formed. No droplets generation or vapor generation are included in the modeling. Droplets are imposed as part of the boundary condition of a gas jet. Droplets transport mechanics and their interaction and momentum exchange with the gas current is made using droplet interaction models as for example Disperse Model (DDM). Geometrical aspects as nozzle dimension, as well as, turbulent model used have a large impact on the core region length of the velocity profile. The numerical results are compared based on the centerline or cross section velocity profiles [53].

In general, centerline, the temperature profile presents an initial decay from the exit of the nozzle until a certain distance, where a minimum value is achieved presumably connected with the location of cessation of boiling and completion of nucleation as main interaction mechanics of energy exchange. After that point, mechanical and evaporation mechanisms become the main driving mechanisms for energy exchange instead. The position at which the minimum temperature occurs is known as Minimum Temperature Distance (MTD). Previous works have not reported major observations on this particular parameter. However, other related concepts as Cold Spray Distance (CSD), which refers to the spray distance where the spray maintains a specific temperature considered “cold” and the Spray Thermal Length (STL) refers to a total spray length where liquid droplets exist [54]. Similar behavior of the temperature profiles at the centerline has been observed in several experimental settings [55–58].

Geometrical characteristics as diameter of the nozzle, length of the nozzle in the experimental system have influence on the dynamics behavior of the system, driving the velocity profile as well as the temperature profile. Evaporation and convection processes are also involved and their relevance along the leaking fluid properties as well as the characteristics of the jet is not well determined yet. Even so, in more recent works, some authors applied the jump condition analysis to the shock waves in the discharge of a superheated liquid [59]. Due to the metastable liquids supply the energy stored within them via the latent heat of vaporization, the evaporation wave was assumed as an adiabatic phase transition.

4.2. Identification of key parameters for sensing technology: viability for sensing based on the concept

As direct consequence of the understanding of the process, it is possible to evaluate the potential of different variables or parameters to detect in the best possible way any leak, keeping in mind that the primary purpose of leak detection systems is to assist pipeline operators in detecting and locating leaks. The first aspect to consider is the magnitudes of the scale of mass discharge, the critical explosion limits, change in temperature of the surrounding, the time scale of the process, or any other parameters that be used to catch this phenomenon. Mass discharge directly seems to be no a convenient parameter to be measured directly but based on the amount of mass going out concentration of the leaked fluid in the surrounding will change. As described, this variable will depend on several physical parameters such as pressure difference, temperature, and fluid properties that will determine the discharge velocity.

Time scale of the leak is related with the jet velocity; however, the thermodynamics process of phase change are under the influence of another parameter as the fluid properties, which can be described based on the temperature variation along the centerline of the jet. Initially, there is a time lag of the initiation of flashing, followed by a drop of temperature driven by a phenomenon of sudden change of phase and finally an increment of the temperature to the ambient condition driven mainly by the mechanics mechanism of energy exchange. Characteristics of centerline droplets temperature of a R134a flashing jet by using and exponential function, which started with an almost exponential decay with the fastest drop in the temperature taking place near the nozzle exit, explained by the presence of rapid evaporation of the droplets and the insufficiency of the convective heat transfer from the surrounding [54]. This exponential decay of droplets average temperature can be described by an exponential function followed by less rapid temperature decay. Meanwhile, experimental data have pointed out that for different substances that there is a visible minimum in the temperature profile that can be related with the factor the mechanics mechanisms take over the thermodynamics mechanics of energy exchange [60]. Mentioned time scales are not commonly reported, however, it is possible to be calculated using the equilibrium model [61].

A different approach described that the flashing process can be detected based on the fact that rapid vaporization or phase change of superheated fluid produced an acoustic pulse that can detect by an acoustic sensor [62, 63]. Nucleation of vapor bubble requires a minimum amount of energy related to the vibrating media that will be traduced in pressure waves (noises). As mentioned in Section 3, the ceramics porous materials (e.g., catalytic and MOS sensors) are other available options for sensing hydrocarbon vapors and this will be discuss in details on the next section.

5. Porous ceramic materials (micro- and nano-materials) for sensing hydrocarbons

Wherever there is a leak at a hydrocarbon facility (e.g., pipeline), there will be hydrocarbon vapors that may be detected. *In situ* detection of hydrocarbon plumes from leakages involves reading of a variety of environmental variables and combination of techniques that will allow to detect the leak in the air, soil, or water. When a gaseous hydrocarbon leak takes place and it migrates to the environment; this would require an immediate detection procedure of hydrocarbon vapors in order to take the respective actions to control any catastrophic accident. This section extensively reviews the recent development of porous ceramic gas sensor materials for hydrocarbon gas leaks including LPG [64, 65], CH_4 [66–68], H_2 [69–71], ethanol [29, 84–88], methanol [89–92], and associated gases such as NO_2 [41, 73–77], H_2S [78–83], and CO [72]. Basically, the discussion will be focused on the specific overlapped section between three interesting areas such as (1) porous ceramic materials, (2) hydrocarbon gas leaks detection, and (3) sensor materials giving the opportunity to explore the interesting niche area for sensing hydrocarbons and their associated gases leaks by porous ceramic materials. In addition, promising materials for sensitive detection of diverse hydrocarbons and/or their associated gases have been identified and are summarized in **Table 2**.

The detection effectivity of hydrocarbons gases by porous ceramic sensor materials (e.g., metal-oxide semiconductor—MOS) have a great influence on the chemical composition of the ceramics, the doping type by specific elements, the porosity type, how morphology-affect the gas sensing properties, etc. According to the information in **Table 2**, the most used porous ceramic materials for hydrocarbon sensing application are (1) the porous tin oxide (SnO_2) which have been applied to detect LPG, methane, H_2 , NO_2 , ethanol, methanol, toluene, etc.; (2) the porous indium oxide (In_2O_3) that shows a great potential to sensing ethanol, methanol and other associated gases to the hydrocarbon field such as NO_2 , H_2S , etc.; and (3) the porous zinc oxide (ZnO) that has been used to sensing ethanol, acetone, NO_2 , H_2S , etc. On the other hand, the catalyst elements mostly used as doping materials in order to improve the sensing properties of the porous ceramics are palladium (Pd) [65, 66, 85], gold (Au) [77], tungsten (W) [76, 95], vanadium (V) [71], cerium (Ce) [90], platinum (Pt) [69], and/or combinations thereof [70, 76, 91]. The Pd could be used to explain the principle of operation of these doping elements which is based on the fact that Pd is a catalytic metal that dissociates the ambient gas to ions. These travel by diffusion to the metal-oxide interface where an electrically polarized layer is formed (according to the ambient gas used). This layer stimulates a change in the electrical characteristics of the MOS device, and hence a sensing mechanism is established [97]. In addition, other compounds such as Sb_2O_5 [41], NiO [70], and graphene [88] have been also evaluated as doping or as secondary materials in advanced composite sensors.

There are only few papers devoted to investigation of sensor properties of porous ceramic materials toward low temperature at high humidity sensing conditions. As humidity is a permanent environmental factor, its control and measurement are particularly important not only for human comfort but also for many industries and technologies. It has been found that the ambient humidity plays a crucial role in the response of the porous ceramic materials based sensor to different hydrocarbons and their associated gases at room temperature. Therefore,

Substance	Porous ceramic materials	Reference
LPG	SnO ₂ nanoflowers and porous nanospheres	[64]
	Porous nanoparticles of α -Fe ₂ O ₃ doped with Pd	[65]
Methane (CH ₄)	Mesoporous SnO ₂ doped with Pd	[66]
	Porous Ga ₂ O ₃	[67]
	Nanoporous SnO ₂	[68]
H ₂	Pt-WO ₃ porous composite ceramics	[69]
	Porous SiO ₂ films doped with NiO and Au nanocrystals	[70]
	Vanadium-doped SnO ₂ oxide porous nanofibers	[71]
CO	SnO ₂ coated with amorphous microporous Si-B-C-N layers	[72]
NO ₂	Mesoporous In ₂ O ₃ nanospheres	[73]
	Sb ₂ O ₅ modified SnO ₂ porous nanocomposites	[41]
	CuO/p-porous silicon	[74]
	Porous corundum-type In ₂ O ₃ nanosheets	[75]
	W- and V-modified mesoporous MCM-41 SiO ₂	[76]
	Au-functionalized porous ZnO nanosheets	[77]
H ₂ S	Porous In ₂ O ₃ nanotubes and nanowires	[78]
	Porous ZnO nanosheet-built network film	[79]
	CuO nanostructures with porous nanosheets	[80]
	In ₂ O ₃ micro/nanostructured porous thin film	[81]
	Porous ZnFe ₂ O ₄ nanosheets	[82]
	Porous α -Fe ₂ O ₃	[83]
Ethanol (C ₂ H ₆ O)	Porous SnO ₂ hollow nanospheres	[84]
	Porous indium oxide (In ₂ O ₃) nanostructured with Pd	[85]
	Porous ZnO-Co ₃ O ₄ hollow polyhedrons heterostructures	[86]
	Mesoporous nickel oxides nanowires	[29]
	Mesoporous Co ₃ O ₄ nanoneedle arrays	[87]
	Mesoporous In ₂ O ₃ -reduced graphene oxide (rGO)	[88]
Methanol (CH ₃ OH)	Porous hierarchical SnO ₂	[89]
	Ce-doped In ₂ O ₃ porous nanospheres	[90]
	Pd-Pt-In ₂ O ₃ composited nanocrystalline SnO ₂	[91]
	Macropore and mesopore SnO ₂	[92]
Toluene (C ₇ H ₈)	Porous Pd-loaded flower-like SnO ₂ microspheres	[93]
	Cr ₂ O ₃ porous microspheres	[94]
Acetone (C ₃ H ₆ O)	Porous WO ₃ -Cr ₂ O ₃ thin films	[95]
	Porous ZnO crystals	[96]

Table 2. Porous ceramic materials for hydrocarbon leaks detection.

ceramic metal oxides are found to be a good choice as humidity sensing materials due to their properties such as high mechanical strength, good physical and chemical stabilities, fast response and recovery times, and wide range of operating temperatures. Semiconducting metal oxide sensors are the widely studied chemiresistive sensors. Recently, nanostructures of semiconductor metal oxides have received considerable interest in the fabrication of humidity and gas sensors due to their high surface-to-volume ratio of atoms, excellent surface reactivity, and the ability to tailor their surface and charge transport properties. Hence, they are considered as ideal candidates as humidity sensors. SnO_2 nanowires, ZrO_2 nanorods, Al_2O_3 nanowires, TiO_2 nanotubes, BaTiO_3 nanofibers, ZnSnO_3 nanocubes, among others constitute the recently explored nanostructured metal oxides to this effect [98].

Tin oxide (SnO_2) is the most versatile oxide used as porous ceramics for sensing hydrocarbon leaks and/or their associated gases. For instance, Wagner et al. [66] produced mesoporous SnO_2 doped with Pd species to be exposed to different gas mixtures at high temperature (600°C) and simulate long term usage. The Pd oxidation state was directly associated to the resistive change of the SnO_2 sensor at different concentrations of methane gas. An important reduction of Pd(II) to Pd(0) was registered for samples evaluated at 5000 ppm of methane in air. The resistive response is affected by the temperature 300°C or 600°C evaluated during the test, and the type of gas used, i.e., synthetic air, pure N_2 , etc. On the other hand, Waitz et al. [68] reveals that mesoporous SnO_2 synthesized by structure replication (nanocasting) from ordered mesoporous KIT-6 silica shows a high thermal stability with no structural loss up to 600°C and only minor decrease in specific surface area by 18% at 800°C . In particular, the samples turn out to be much more stable than porous SnO_2 materials prepared by sol-gel-based synthesis procedures for comparison. The thermal stability facilitates the utilization of the materials as sensors for combustible gases showing promising behavior for the methane (CH_4) sensing methodologies. In addition, Ho et al. [64] synthesized SnO_2 with two different microstructures: (1) hierarchical SnO_2 flowers assembled by numerous one-dimensional tetragonal prism nanorods, and (2) SnO_2 sphere architectures formed by numerous smaller particles. The results show that the nanoflowers exhibited higher sensitivities to ethanol than the nanospheres, whereas the typical responses of these sensors to H_2 and LPG indicated that the porous spheres demonstrated better sensing performance than the hierarchical flowers [64]. This research is a main example about how the material's microstructure/morphology could affect the sensing properties of the same material; the results demonstrated the great effect that the microstructures could have on the final gas sensing properties of this metal oxide.

Indium oxide (In_2O_3), as a typical n-type semiconductor with a band gap of 3.55–3.75 eV, has been investigated extensively in last decade for its applications in diverse areas. For instance, Gong et al. [85] successfully synthesized porous In_2O_3 nanocuboids on a large scale and the sensors made with them exhibit enhanced sensitivity and stability to reducing gases including H_2S , acetone, ethanol and methanol vapors, after modified with Pd nanoparticles. The results indicate the existence of abundant pores for the aggregations of particles in the materials. The BET surface area of the materials is $36.2 \text{ m}^2 \text{ g}^{-1}$. As was mentioned, the In_2O_3 and $\text{Pd@In}_2\text{O}_3$ nanocuboids were used to produce two different types of chemical sensors. The sensor fabricated with $\text{Pd@In}_2\text{O}_3$ was more stable with a higher response to the reducing vapors

in comparison to the In_2O_3 nanocuboids sensor. The results also indicate that Pd nanoparticles have a positive effect on the sensing mechanism of In_2O_3 nanocuboids. On the other hand, hydrogen sulfide (H_2S) is a toxic, flammable, colorless, and malodorous gas that has been getting strong attention in the industrial gases sensing field for several years. Therefore, In_2O_3 -based sensing film and its sensing performances to H_2S (especially at low working temperature) have been much studied and received superior attentions [99]. In the same order of idea, In_2O_3 nanoparticle film synthesized by hydrothermal method and studied its gas sensing performances to H_2S at different temperatures above 125°C . Such film exhibited a strong and selective sensing to H_2S at 268°C among the normal gas molecules. In addition, nanocrystalline In_2O_3 -based films had a high response to H_2S gas at 150°C . Also, the nanostructured In_2O_3 thin films, induced by spray pyrolysis technique, showed a good sensitivity to H_2S at a lower temperature of 50°C [99]. Wang et al. [99] reported the sensing properties of In_2O_3 micro/nanostructured orderly porous thin film produced by solution-dipping monolayer organic colloidal template. This sensing material was used for H_2S detection at room temperature. The results indicated that the humidity has a great effect on the sensing properties of the In_2O_3 porous film where H_2S was not detected in ambient without humidity. This sensing material shows an ultra-high response value to H_2S at room temperature with a significant humidity-induced enhanced sensing performance. The results also indicate that the sensing mechanism of the In_2O_3 film for the H_2S at room temperature is due to three potential effect such as (1) the ambient humidity-induced H_2S hydrolyzation, (2) the hydrolyzation-induced desorption of the chemisorbed oxygen and adsorption of water, or (3) even formation of water thin film on the In_2O_3 surface produced by the effect of the ambient humidity. This research team also proposed a design of an In_2O_3 porous thin film-based sensor array with potential uses for the H_2S detection under environmental operational conditions.

Zinc oxide (ZnO) is one of the most auspicious materials for a large number of applications because of its physicochemical properties, where its chemical sensitivity permits to be used as a sensing material for many gases including H_2 , NO_2 , O_2 , $\text{CH}_3\text{CH}_2\text{OH}$, NH_3 , and LPG [100]. Accordingly, Al-Salmana et al. [100] produced ZnO nanostructure deposited on the PET and quartz substrates, and found that ZnO sensor based on PET substrate has a sensitivity value of 24.8% for H_2 gas tested at room temperature with an increase until 99.53% at 200°C with a response of 224. Otherwise, ZnO sensor based on quartz substrate showed high sensitivity (96.29%) at 100°C , with an increase until 99.95% at 250°C and a response value of 2254. The ZnO gas sensors based on PET and quartz substrates showed high sensitivity, stability, and recovery to the initial value of the sensor signal when they were operating at temperatures between 100 and 200°C . These sensing materials used for H_2 gas detection and based on ZnO nanostructures were stable over several cycles and had a fast response at different operating temperatures. On the other hand, Wagner et al. [101] produced mesoporous ZnO and evaluated its sensing properties for CO and NO_2 detection in a concentration range of 2–10 ppm at a relative humidity of 50%. It is well known that the long-term permit-exposure values for the human race without health damage are about 30 ppm for CO and 5 ppm for the NO_2 . This research group indicated that their mesoporous sensing materials can be used for the detection of these gases under concentration below of the legal thresholds register in most countries and showed previously.

Other kind of porous ceramics materials have been investigated for hydrocarbons gases detection. For instance, Picasso et al. [65] have produced sensors based on nanoparticles of $\alpha\text{-Fe}_2\text{O}_3$ doped with different amounts of Pd ranging from 0.1 to 1.0 wt.% for liquefied petroleum gas (LPG) detection. They demonstrated that the sample of Pd-doped sensors showed much higher sensitivity than the undoped one revealing the promotion electronic effect of Pd^{2+} on the surface reaction. Among all samples, the sensor with 0.75 wt.% Pd presented the highest gas response at 300°C in all gas tested concentrations, likely due to the highest BET surface, well-defined hematite crystalline structure and best surface contact over Pd surface via electronic mechanism. On the other hand, Xiaoqing Li et al. [29] produced mesoporous NiO NWs by using SBA-15 silica as the hard templates with the nanocasting method under the calcination temperature between 550 and 750°C . All results showed that all samples exhibited the best response to ethanol gas. The specific surface area decreased with the increasing calcination temperature, while crystallization degree and bandgap increased. Owing to the suitable specific surface area, crystallization degree and bandgap at the calcination temperature of 650°C , mesoporous NiO NWs-650 exhibited the best gas-sensing performance. For ethanol detection Co_3O_4 nanoneedle arrays were successfully fabricated via a facile two-step approach, including the formation of needle-shaped $\text{Co}(\text{CO}_3)0.5(\text{OH})\cdot 0.11\text{H}_2\text{O}$ followed by thermal conversion to mesoporous Co_3O_4 . The highest sensitivity reached ~ 89.6 for 100 ppm ethanol vapor and the optimal working temperature was as low as 130°C [87].

In addition, some of the most sensing materials used for humidity conditions are based on metal oxides, spinel- and perovskite-type oxides and/or thereof combination. Basically, the physicochemical properties of these materials allow them to detect humidity in gaseous media. The sensing mechanism of ceramic humidity sensors is based on water adsorption on the ceramic surface. The microstructure of these ceramic materials integrated by grains, porous, and their crystalline or non-crystalline phases support the sensing mechanism process. Hence, these kinds of sensors are based on the mechanical or electrical change due to bulk and/or surface modifications of the sensing materials with water adsorption [102]. Finally, the present state-of-art indicates that there are just a few publications related to the sensing hydrocarbons and/or their associated gases at low temperature and high humidity indicating a great niche for future researches.

6. Conclusion

In the recent past, a great deal of research efforts were directed toward the development of advanced ceramics porous materials due to their sensing properties and potential application for sensing hydrocarbons and/or their associated gases leaks. Among the various techniques that are available for gas detection, solid state metal oxides offer a wide spectrum of materials and their sensitivities for different gaseous species, making it a better choice over other options. The oxides that are covered in this study include oxides of aluminum, silicon, bismuth, cerium, chromium, cobalt, copper, indium, iron, nickel, niobium, tin, titanium, tungsten, vanadium, zinc, zirconium, and the mixed or multi-component metal oxides. The cover hydrocarbons and their associated gases are liquefied petroleum gas (LPG), CH_4 , ethanol ($\text{C}_2\text{H}_6\text{O}$), methanol (CH_3OH), acetone ($\text{C}_3\text{H}_6\text{O}$), H_2 , NH_3 , CO , H_2S , NO_x , among others.

The book chapter mentions the principle of the hydrocarbon leaks and the advances in the production and applications of micro- and nanoporous ceramics for hydrocarbon leaks under diverse environmental conditions (e.g., humidity and low temperatures) that also affects the sensing capability of these materials. Finally, sensing of hydrocarbon leaks at low temperatures and high humidity conditions is clearly identified as niche area that requests future research efforts.

Acknowledgements

Dr. Y.A. Perera-Mercado is grateful to the West Houston Center for Science and Engineering Center (WHC) at Houston Community College System (HCCS); and Dr. G. Castruita-de Leon is thankful to Cátedras-CONACYT for the support received from both organizations in order to write this book chapter. Finally, the publication charges for this article have been funded by a grant from the publication fund of UiT The Arctic University of Norway.

Author details

Yibran A. Perera-Mercado^{1*}, Griselda Castruita-de Leon² and Geanette Polanco Piñerez³

*Address all correspondence to: yibranpereramercado@gmail.com

1 West Houston Center for Science & Engineering (WHC) at Houston Community College System (HCCS), Houston, Texas, USA

2 CONACYT—Research Center for Applied Chemistry (CIQA), Saltillo, Coahuila, México

3 The Arctic University of Norway, Faculty of Engineering and Technology, Institute of Industrial Technology, Narvik, Norway

References

- [1] Salmasi SSZ, Abbas-Abadi MS, Haghighi MN, Abedini H. The effect of different zeolite based catalysts on the pyrolysis of polybutadiene rubber. *Fuel*. 2015;**160**:544-548. DOI: 10.1016/j.fuel.2015.07.091
- [2] Sahnner K, Hagen G, Schönauer S, Reiß S, Moos R. Zeolites-versatile materials for sensors. *Solid State Ionics*. 2008;**179**:2416-2423. DOI: 10.1016/j.ssi.2008.01.024
- [3] Masoudi-Nejad M, Fatemi S. Thermodynamic adsorption data of CH₄, C₂H₆, C₂H₄ as the OCM process hydrocarbons on SAPO-34 molecular sieve. *Journal of Industrial and Engineering Chemistry*. 2014;**20**:4045-4053. DOI: 10.1016/j.jiec.2013.12.107
- [4] Boyjoo Y, Wang M, Pareek VK, Liu J, Jaroniec M. Synthesis and application of porous non-silica metal oxides submicrospheres. *Chemical Society Reviews*. 2016;**45**:6013-6047. DOI: 10.1039/c6cs00060f

- [5] Anbia M, Koohsaryan E, Borhani A. Novel hydrothermal synthesis of hierarchically-structured zeolite LTA microspheres. *Materials Chemistry and Physics*. 2017;**193**: 380-390. DOI: 10.1016/j.matchemphys.2017.02.048
- [6] Snelders DJM, Valega Mackenzie FO, Boersma A, Peeters RHM. Zeolites as coating materials for Fiber Bragg Grating chemical sensors for extreme conditions. *Sensors and Actuators B*. 2016;**235**:689-706. DOI: 10.1016/j.snb.2016.05.133
- [7] Cheng XW, Meng QY, Chen JY, Long YC. A facile route to synthesize mesoporous ZSM-5 zeolite incorporating high ZnO loading in mesopores. *Microporous and Mesoporous Materials*. 2012;**153**:198-203. DOI: 10.1016/j.micromeso.2011.12.041
- [8] Deng X, Zhang L, Guo J, Chen Q, Ma J. ZnO enhanced NiO-based gas sensors towards ethanol. *Materials Research Bulletin*. 2017;**90**:170-174. DOI: 10.1016/j.materresbull.2017.02.040
- [9] Vilaseca M, Coronas J, Cirera A, Cornet A, Morante JR, Santamaria J. Gas detection with SnO₂ sensors modified by zeolite films. *Sensors and Actuators B*. 2007;**124**:99-110. DOI: 10.1016/j.snb.2006.12.009
- [10] Varsani P, Afonja A, Williams DE, Parkin IP, Binions R. Zeolite-modified WO₃ gas sensors-enhanced detection of NO₂. *Sensors and Actuators B*. 2011;**160**:475-482. DOI: 10.1016/j.snb.2011.08.014
- [11] Hagen G, Dubbe A, Retting F, Jerger A, Birkhofer T, Müller R, Plog C, Moos R. Selective impedance based gas sensors for hydrocarbons using ZSM-5 zeolite films with chromium (III) oxide interface. *Sensors and Actuators B*. 2006;**119**:441-448. DOI: 10.1016/j.snb.2005.12.052
- [12] Tarttelin-Hernández P, Hailes SMV, Parkin IP. Hydrocarbon detection with metal oxide semiconducting gas sensors modified by overlayer or admixture of zeolites Na-A, H-Y and H-ZSM-5. *Sensors and Actuators B*. 2017;**242**:1281-1295. DOI: 10.1016/j.snb.2016.09.000
- [13] Mir MA, Bhat MA, Naikoo RA, Bhat RA, Khan M, Shaik M, Kumar P, Sharma PK, Tomar R. Utilization of zeolite/polymer composites for gas sensing: A review. *Sensors and Actuators B*. 2017;**242**:1007-1020. DOI: 10.1016/j.snb.2016.09.152
- [14] Olad A, Khatamian M, Naseri B. Preparation of polyaniline nanocomposite with natural clinoptilolite and investigation of its special properties. *International Journal of Nanoscience and Nanotechnology*. 2010;**6**:43-52
- [15] Sun B, Zhou G, Zhang H. Synthesis, functionalization and applications of morphology-controllable silica-based nanostructures: A review. *Progress in Solid State Chemistry*. 2016;**44**:1-19. DOI: 10.1016/j.progsolidstchem.2016.01.001
- [16] Fakoya MF, Shah SN. Emergence of nanotechnology in the oil and gas industry: Emphasis on the application of silica nanoparticles, In *Petroleum*. 2017;**3**(4):391-405. ISSN 2405-6561. <https://doi.org/10.1016/j.petlm.2017.03.001>
- [17] Rahman IA, Padavettan V. Synthesis of silica nanoparticles by sol-gel: Size-dependent properties, surface modification, and applications in silica-polymer nanocomposites—A review. *Journal of Nanomaterials*. 2012:1-15. DOI: 10.1155/2012/132424

- [18] Meléndez-Ortiz HI, Mercado-Silva A, García-Cerda LA, Castruita G, Perera-Mercado YA. Hydrothermal synthesis of mesoporous silica MCM-41 using commercial sodium silicate. *Journal of the Mexican Chemical Society*. 2013;**57**:73-79
- [19] Meléndez-Ortiz HI, Puente-Urbina B, Castruita-de León G, Mata-Padilla JM, García-Uriostegui L. Synthesis of spherical SBA-15 mesoporous silica. Influence of reaction conditions on the structural order and stability. *Ceramics International*. 2016;**42**:7564-7570. DOI: 10.1016/j.ceramint.2016.01.163
- [20] Golezani AS, Fateh AS, Mehrabi HA. Synthesis and characterization of mesoporous silica material produced by hydrothermal continuous pH adjusting path way. *Progress in Natural Science*. 2016;**26**:411-414. DOI: 10.1016/j.pnsc.2016.07.003
- [21] Yang L, Wu H, Jia J, Ma B, Li J. Synthesis of bimodal mesoporous silica with coexisting phases by co-hydrothermal aging route with P123 containing gel and F127 containing gel. *Microporous and Mesoporous Materials*. 2017;**253**:151-159. DOI: 10.1016/j.micromeso.2017.06.037
- [22] Dudarko OA, Gunathilake C, Sliesarenko VV, Zub YL, Jaroniec M. Microwave-assisted and conventional hydrothermal synthesis of ordered mesoporous silicas with P-containing functionalities. *Colloids and Surfaces, A: Physicochemical and Engineering Aspects*. 2014;**459**:4-10. DOI: 10.1016/j.colsurfa.2014.06.036
- [23] Meléndez-Ortiz HI, Perera-Mercado YA, García-Cerda LA, Mercado-Silva JA, Castruita G. Influence of the reaction conditions on the thermal stability of mesoporous MCM-48 silica obtained at room temperature. *Ceramics International*. 2014;**40**:4155-4161. DOI: 10.1016/j.ceramint.2013.08.072
- [24] Meléndez-Ortiz HI, García-Cerda LA, Olivares-Maldonado Y, Castruita G, Mercado-Silva JA, Perera-Mercado YA. Preparation of spherical MCM-41 molecular sieve at room temperature: Influence of the synthesis conditions in the structural properties. *Ceramics International*. 2012;**38**:6353-6358. DOI: 10.1016/j.ceramint.2012.05.007
- [25] Castruita-de León G, Perera-Mercado YA, García-Cerda LA, Mercado-Silva JA, Meléndez-Ortiz HI, Olivares-Maldonado Y, Alvarez-Contreras L. Synthesis of amino-functionalized MCM-48 silica via direct co-condensation at room temperature. *Microporous and Mesoporous Materials*. 2015;**204**:156-162. DOI: 10.1016/j.micromeso.2014.11.023
- [26] Amonette JE, Matyás J. Functionalized silica aerogels for gas-phase purification, sensing, and catalysis: A review. *Microporous and Mesoporous Materials*. 2017;**250**:100-119. DOI: 10.1016/j.micromeso.2017.04.055
- [27] Xiao L, Grogan MDW, Wadsworth WJ, England R, Birks TA. Stable-low optical nanofibers embedded in hydrophobic aerogel. *Optics Express*. 2011;**19**:764-770
- [28] El-Nahhal IM, Salem JK, Kuhn S, Hammad T, Hempelmann R, Al Bhaisi S. Synthesis & characterization of silica coated and functionalized silica coated zinc oxide nanomaterials. *Powder Technology*. 2016;**287**:439-446. DOI: 10.1016/j.powtec.2015.09.042

- [29] Li X, Li D, Xu J, Jin H, Jin D, Peng X, Hong B, Li J, Yang Y, Ge H, Wang X. Calcination-temperature-dependent gas-sensing properties of mesoporous nickel oxides nanowires as ethanol sensors. *Powder Technology*. 2017;**318**:40-45. DOI: 10.1016/j.powtec.2017.05.020
- [30] Kita J, Schubert F, Retting F, Engelbrecht A, Groß A, Moos R. Ceramic alumina substrates for high-temperature gas sensors-implications for applicability. *Procedia Engineering*. 2014;**87**:1005-1508. DOI: 10.1016/j.proeng.2014.11.584
- [31] Castruita G, Perera-Mercado YA, Saucedo-Salazar EM. Sol-gel aluminum hydroxides and their thermal transformation studies for the production of α -alumina. *Journal of Inorganic and Organometallic Polymers*. 2013;**23**:1145-1152. DOI: 10.1007/s10904-013-9905-y
- [32] Hyodo T, Hashimoto T, Ueda T, Nakagoe O, Kamada K, Sasahara T, Tanabe S, Shimizu Y. Adsorption/combustion-type VOC sensors employing mesoporous γ -alumina co-loaded with noble-metal and oxide. *Sensors and Actuators B*. 2015;**220**:1091-1104. DOI: 10.1016/j.snb.2015.06.065
- [33] Sharma K, Islam SS. Optimization of porous anodic alumina nanostructure for ultra-high sensitive humidity sensor. *Sensors and Actuators B*. 2016;**237**:443-451. DOI: 10.1016/j.snb.2016.06.041
- [34] Norek M, Stepniowski WJ, Polński M, Zasada D, Bojar Z, Bystrzycki JA. Comparative study on the hydrogen absorption of thin films at room temperature deposited on non-porous glass substrate and nano-porous anodic aluminum oxide (AAO) template. *Inter. J. Hydrogen Energy*. 2011;**36**:11777-11784. DOI: 10.1016/j.ijhydene.2011.06.046
- [35] Mozalev A, Calavia R, Vázquez RM, Gracia I, Cané C, Correig X, Vilanova X, Gispert-Guirado F, Hubálek J, Llobet E. MEMS-microhotplate-based hydrogen gas sensor utilizing the nanostructured porous-anodic-alumina-supported WO_3 active layer. *International Journal of Hydrogen Energy*. 2013;**38**:8011-8021. DOI: 10.1016/j.ijhydene.2013.04.063
- [36] MSA Safety Company. Gas Detection Handbook. Key Concepts & Reference Materials for Permanently Installed Gas-monitoring Systems. 5th ed. US: MSA Instrument Division; 2007. 145 p
- [37] Maduraiveeran G, Jin W. Nanomaterials based electrochemical sensor and biosensor platforms for environmental applications. *Trends in Environmental Analytical Chemistry*. 2017;**13**:10-23. DOI: 10.1016/j.teac.2017.02.001
- [38] Fergus JW. Solid electrolyte based sensor for measurement of CO and hydrocarbon gases. *Sensors and Actuators B*. 2007;**122**:683-693. DOI: 10.1016/j.snb.2006.06.024
- [39] Xinxin X, Chen T, Zhao R, Wang Z, Wang Y. A low temperature butane gas sensor used Pt nanoparticles-modified AZO macro/mesoporous nanosheets as sensing material. *Sensors and Actuators B*. 2018;**254**:227-238. DOI: 10.1016/j.snb.2017.07.091
- [40] Xu H, Zhang J, Rehman AU, Gong L, Kan K, Li L. Synthesis of NiO@CuO nanocomposites as high-performance gas sensing for NO_2 at room temperature. *Applied Surface Science*. 2017;**412**:230-237. DOI: 10.1016/j.apsusc.2017.03.213

- [41] Ni Y, Du W, Fang W, Chen X, Liu W, Wang Y, Liu J. High response to nitrogen dioxide derived from antimony peroxide modified tin oxide porous nanocomposites serving as gas sensing material. *Sensors and Actuators B*. 2017;**247**:216-223. DOI: 10.1016/j.snb.2017.03.019
- [42] Hung CM, Hoa ND, Duy NV, Toan NV, Le DTT, Hieu NV. Synthesis and gas-sensing characteristics of α -Fe₂O₃ hollow balls. *Journal of Science: Advanced Materials and Devices*. 2016;**1**:45-50. DOI: 10.1016/j.jsamd.2016.03.003
- [43] Wongrat E, Chanlek N, Chueaiarrom C, Samransuksamer B, Hongstith N, Choopun S. Low temperature ethanol response enhancement of ZnO nanostructures sensors decorated with gold nanoparticles exposed to UV illumination. *Sensors and Actuators B*. 2016;**251**:188-197. DOI: 10.1016/j.sna.2016.10.022 0924-4247
- [44] Karaduman I, Er E, Celikkan H, Erk N, Acar S. Room-temperature ammonia gas sensor based on reduced graphene oxide nanocomposites decorated by Ag, Au and Pt nanoparticles. *Journal of Alloys and Compounds*. 2017;**722**:569-578. DOI: 10.1016/j.jallcom.2017.06.152
- [45] Liu L, Song P, Wei Q, Yang Z, Wang Q. Synthesis of porous SnO₂ hexagon nanosheets loaded with Au nanoparticles for high performance gas sensor. *Materials Letters*. 2017;**201**:211-215. DOI: 10.1016/j.matlet.2017.05.024
- [46] Zhang B, Li M, Song Z, Kan H, Yu H, Liu Q, Zhang G, Liu H. Sensitive H₂S gas sensor employing colloidal zinc oxide quantum dots. *Sensors and Actuators B*. 2017;**249**:558-563. DOI: 10.1016/j.snb.2017.03.098
- [47] Balamurugan C, Lee DW, Maheswari AR, Parmar M. Porous wide band gap BiNbO₄ ceramic nanopowder synthesized by low temperature solution-based method for gas sensing applications. *RSC Advances*. 2014;**4**:54625-54630. DOI: 10.1039/c4ra08898k
- [48] Authority PS. Petroleum Safety Authority Norway [Internet]. 2017. Available from: <http://www.psa.no/risk-level/category876.html> [Accessed: 2016-06-15]
- [49] Abbasi T, Abbasi SA. Accidental risk of superheated liquids and a framework for predicting the superheat limit. *Journal of Loss Prevention in the Process Industries*. 2007;**20**:165-181. DOI: 10.1016/j.jlp.2005.11.002
- [50] Polanco G. Phase Change within Flows from Breaches of Liquefied Gas Pipelines. Coventry, UK: Coventry University; 2008
- [51] Deaves DM, Gilham S, Mitchell BH, Woodburn P, Shepherd AM. Modelling of catastrophic flashing releases. *Journal of Hazardous Materials*. 2001;**88**(1):1-32. DOI: 10.1016/S0304-3894(01)00284-9
- [52] Demichela M, Piccinini N, Poggio A. Analysis of an LPG accidental release. *Safety and Environmental Protection*. 2004;**82**(2):128-131. DOI: 10.1205/095758204322972762
- [53] Polanco G, Holdo AE, Munday AG. General review of flashing jet studies. *Journal of Hazardous Materials*. 2010;**173**:2-18. DOI: 10.1016/j.jhazmat.2009.08.138

- [54] Zhifu Z, Weitao W, Bin C, Guoxiang W, Liejin G. An experimental study on the spray and thermal characteristics of R134a two-phase flashing spray. *International Journal of Heat and Mass Transfer*. 2012;**55**:4460-4468. DOI: 10.1016/j.ijheatmasstransfer.2012.04.021
- [55] Allen JT. *Laser-based Velocity Measurement in Two-phase Flashing Propane Jet Releases*. Health and Safety Laboratory; 1996
- [56] Allen JT. *Laser-based Droplet Size measurements in Two-phase, Flashing Propane Jets*. Health and Safety Laboratory; 1996
- [57] Allen JT. *Laser-Based Measurements in two-Phase Flashing Propane Jets*. University of Sheffield; 1998
- [58] Yildiz D, Rambund P, Van Beeck JPJA, Buchlin J-M. Thermal characterization of a R134A two-phase flashing jet. In: *ICLASS 2003—9th International Conference on Liquid Atomization and Spray Systems*; July 2003; Sorrento, Italy
- [59] Moreira JRS, Bullard CW. Pressure drop and flashing mechanisms in refrigerant expansion devices. *International Journal of Refrigeration*. 2003;**26**:840-848. DOI: 10.1016/S0140-7007(03)00070-7
- [60] Yildiz D, Beeck JPJA, Riethmuller ML. Global rainbow thermometry applied to a flashing two-phase R134-A Jet. In *11th International Symposium on Application of Laser Techniques to Fluid Mechanics*; 2002; Lisbon, Portugal
- [61] Friedel SKL. Assessment of the maximum possible liquid superheat during flashing leak flow. *Journal of Loss Prevention in the Process Industries*. 1997;**10**(54):345-350
- [62] Sarkar R, Mondal PK, Chatterjee BK. Study of acoustic emission due to vaporisation of superheated droplets at higher pressure. *Physics Letters A*. 2017;**381**:2531-2537
- [63] Mondal PK, Sarkar R, Chatterjee BK. Response of superheated droplet detector (SDD) and bubble detector (BD) to interrupted irradiations. *Nuclear Instruments and Methods in Physics Research A*. 2017;**857**:111-114
- [64] Ho LT, Cuong ND, Hoa TT, Khieu DQ, Long HT, Quang DT, Hoa ND, Hieu NV. Synthesis, characterization, and comparative gas sensing properties of tin dioxide nanoflow-ers and porous nanospheres. *Ceramics International*; **10**:14819-14825. DOI: 10.1016/j.ceramint.2015.08.003
- [65] Picasso G, Sun Kou MR, Vargasmachuca O, Rojas J, Zavala C, Lopez A, Irusta S. Sensors based on porous Pd-doped hematite ($\alpha\text{-Fe}_2\text{O}_3$) for LPG detection. *Microporous and Mesoporous Materials*. 2014;**185**(1):79-85. DOI: 10.1016/j.micromeso.2013.11.014
- [66] Wagner T, Bauer M, Sauerwal T, Kohl CD, Tiemann M. X-ray absorption near-edge spectroscopy investigation of the oxidation state of Pd species in nanoporous SnO_2 gas sensors for methane detection. *Thin Solid Films*. 2011;**520**(3):909-912. DOI: 10.1016/j.tsf.2011.04.187

- [67] Flingelli GK, Fleischer MM, Meixner H. Selective detection of methane in domestic environments using a catalyst sensor system based on Ga_2O_3 . *Sensors and Actuators B: Chemical*. 1998;**48**(1-3):258-262. DOI: 10.1016/S0925-4005(98)00054-9
- [68] Waitz T, Becker B, Wagner T, Sauerwald T, Kohl C-D, Tiemann M. Ordered nanoporous SnO_2 gas sensors with high thermal stability. *Sensors and Actuators B: Chemical*. 2010;**150**(2):788-793. DOI: 10.1016/j.snb.2010.08.001
- [69] Song C, Wu G, Sun B, Xiong Y, Zhu S, Hu Y, Gu H, Wang Y, Chen W. Pt- WO_3 porous composite ceramics outstanding for sensing low concentrations of hydrogen in air at room temperature. *International Journal of Hydrogen Energy*. 2017;**42**(9):6420-6424. DOI: 10.1016/j.ijhydene.2016.12.101
- [70] Gaspera ED, Busu D, Guglielmi M, Martucci A, Bello V, Mattei G, Post ML, Cantalini C, Agnoli S, Granozzi G, Sadek AZ, Kalantar-Zadeh K, Wlodarski W. Comparison study of conductometric, optical and SAW gas sensors based on porous sol-gel silica films doped with NiO and Au nanocrystals. *Sensors and Actuators B: Chemical*. 2010;**143**(2):567-573. DOI: 10.1016/j.snb.2009.09.060
- [71] Xu X, Yin M, Li N, Wang W, Sun B, Liu M, Zhang D, Li Z, Wang C. Vanadium-doped tin oxide porous nanofibers: Enhanced responsivity for hydrogen detection. *Talanta*. 2017;**167**(15):638-644. DOI: 10.1016/j.talanta.2017.03.013
- [72] Prasad RM, Gurlo A, Riedel R, Hübner M, Barsan N, Weimar U. Microporous ceramic coated SnO_2 sensors for hydrogen and carbon monoxide sensing in harsh reducing conditions. *Sensors and Actuators B: Chemical*. 2010;**149**(1):105-109. DOI: 10.1016/j.snb.2010.06.016
- [73] Xiao B, Wang D, Song S, Zhai C, Wang F, Zhanga M. Fabrication of mesoporous In_2O_3 nanospheres and their ultrasensitive NO_2 sensing properties. *Sensors and Actuators B*. 2017;**248**:519-526. DOI: 10.1016/j.snb.2017.04.022
- [74] Liu X, Hu M, Wang Y, Liu J, Qin Y. High sensitivity NO_2 sensor based on CuO/p-porous silicon heterojunction at room temperature. *Journal of Alloys and Compounds*. 2016;**685**:364-369. DOI: 10.1016/j.jallcom.2016.05.215
- [75] Gao L, Cheng Z, Xiang Q, Zhang Y, Xu J. Porous corundum-type In_2O_3 nanosheets: Synthesis and NO_2 sensing properties. *Sensors and Actuators B*. 2015;**208**:436-443. DOI: 10.1016/j.snb.2014.11.053
- [76] Yuliarto B, Honma I, Katsumura Y, Zhou H. Preparation of room temperature NO_2 gas sensors based on W- and V-modified mesoporous MCM-41 thin films employing surface photovoltage technique. *Sensors and Actuators B: Chemical*. 2006;**114**(1):109-119. DOI: 10.1016/j.snb.2005.04.016
- [77] Mun Y, Park S, An S, Lee C, Kim HW. NO_2 gas sensing properties of Au-functionalized porous ZnO nanosheets enhanced by UV irradiation. *Ceramics International*. 2013;**9**(8):8615-8622. DOI: 10.1016/j.ceramint.2013.04.035

- [78] Xu L, Dong B, Wang Y, Bai X, Liu QQ, Song H. Electrospinning preparation and room temperature gas sensing properties of porous In_2O_3 nanotubes and nanowires. *Sensors and Actuators B: Chemical*. 2010;**147**(2):531-538. DOI: 10.1016/j.snb.2010.04.003
- [79] Zhu Y, Wang Y, Duan G, Zhang H, Li Y, Liu G, Lei X, Cai W. In situ growth of porous ZnO nanosheet-built network film as high-performance gas sensor. *Sensors and Actuators B: Chemical*. 2015;**221**(31):350-356. DOI: 10.1016/j.snb.2015.06.115
- [80] Li Z, Wang J, Wang N, Yan S, Liu W, Qing FY, Wang Z. Hydrothermal synthesis of hierarchically flower-like CuO nanostructures with porous nanosheets for excellent H_2S sensing. *Journal of Alloys and Compounds*. 2017;**725**:1136-1143. DOI: 10.1016/j.jallcom.2017.07.218
- [81] Wang Y, Duan G, Zhu Y, Zhang H, Xu Z, Dai Z, Cai W. Room temperature H_2S gas sensing properties of In_2O_3 micro/nanostructured porous thin film and hydrolyzation-induced enhanced sensing mechanism. *Sensors and Actuators B: Chemical*. 2016;**228**(2):74-84. DOI: 10.1016/j.snb.2016.01.002
- [82] Gao X, Sun Y, Zhu C, Li C, Ouyang Q, Chen Y. Highly sensitive and selective H_2S sensor based on porous ZnFe_2O_4 nanosheets. *Sensors and Actuators B: Chemical*. 2017;**246**:662-672. DOI: 10.1016/j.snb.2017.02.100
- [83] Huang Y, Chen W, Zhang S, Kuang Z, Ao D, Alkurd NR, Zhou W, Liu W, Shen W, Li Z. A high performance hydrogen sulfide gas sensor based on porous $\alpha\text{-Fe}_2\text{O}_3$ operates at room-temperature. *Applied Surface Science*. 2015;**351**:1025-1033. DOI: 10.1016/j.apsusc.2015.06.053
- [84] Qiang Z, Ma SY, Jiao HY, Wang TT, Jiang XH, Jin WX, Yang HM, Chen H. Highly sensitive and selective ethanol sensors using porous SnO_2 hollow spheres. *Ceramics International*. 2016;**42**:8983-18990. DOI: 10.1016/j.ceramint.2016.09.053
- [85] Gong F, Gong Y, Liu H, Zhang M, Zhang Y, Li F. Porous In_2O_3 nanocuboids modified with Pd nanoparticles for chemical sensors. *Sensors and Actuators B*. 2016;**223**:384-391. DOI: 10.1016/j.snb.2015.09.053
- [86] Xiong Y, Xu W, Zhu Z, Xue Q, Lu W, Ding D, Zhu L. ZIF-derived porous $\text{ZnO-Co}_3\text{O}_4$ hollow polyhedrons heterostructure with highly enhanced ethanol detection performance. *Sensors and Actuators B: Chemical*. 2017;**253**:523-532. DOI: 10.1016/j.snb.2017.06.169
- [87] Wen Z, Zhu L, Li Y, Zhang Z, Ye Z. Mesoporous Co_3O_4 nanoneedle arrays for high-performance gas sensor. *Sensors and Actuators B: Chemical*. 2014;**203**:873-879. DOI: 10.1016/j.snb.2014.06.124
- [88] Xue P, Yang X, Lai X, Xia W, Li P, Fang J. Controlling synthesis and gas-sensing properties of ordered mesoporous In_2O_3 -reduced graphene oxide (rGO) nanocomposite. *Science Bulletin*. 2015;**60**(15):1348-1354. DOI: 10.1007/s11434-015-0852-6
- [89] Zhang C, Wang J, Hu R, Qiao Q, Li X. Synthesis and gas sensing properties of porous hierarchical SnO_2 by grapefruit exocarp biotemplate. *Sensors and Actuators B: Chemical*. 2016;**222**:1134-1143. DOI: 10.1016/j.snb.2015.08.016

- [90] Han D, Song P, Zhang S, Zhang H, Xu Q, Wang Q. Enhanced methanol gas-sensing performance of Ce-doped In_2O_3 porous nanospheres prepared by hydrothermal method. *Sensors and Actuators B: Chemical*. 2015;**216**:488-496. DOI: 10.1016/j.snb.2015.04.083
- [91] Li Y, Deng D, Xing X, Chen N, Liu X, Xiao X, Wang YA. High performance methanol gas sensor based on palladium-platinum- In_2O_3 composited nanocrystalline SnO_2 . *Sensors and Actuators B: Chemical*. 2016;**237**:133-141. DOI: 10.1016/j.snb.2016.06.088
- [92] Wang J, Xu Y, Xu W, Zhang M, Chen X. Simplified preparation of SnO_2 inverse opal for methanol gas sensing performance. *Microporous and Mesoporous Materials*. 2015;**208**:93-97. DOI: 10.1016/j.micromeso.2015.01.038
- [93] Tian J, Wang J, Hao Y, Du H, Li X. Toluene sensing properties of porous Pd-loaded flower-like SnO_2 microspheres. *Sensors and Actuators B: Chemical*. 2014;**202**:795-802. DOI: 10.1016/j.snb.2014.05.048
- [94] Ma H, Xu Y, Rong Z, Cheng X, Gao S, Zhang X, Zhao H, Huo L. Highly toluene sensing performance based on monodispersed Cr_2O_3 porous microspheres. *Sensors and Actuators B: Chemical*. 2012;**174**:325-331. DOI: 10.1016/j.snb.2012.08.073
- [95] Gao P, Ji H, Zhou Y, Li X. Selective acetone gas sensors using porous WO_3 - Cr_2O_3 thin films prepared by sol-gel method. *Thin Solid Films*. 2012;**520**(7):3100-3106. DOI: 10.1016/j.tsf.2011.12.003
- [96] Xie X, Wang X, Tian J, Song X, Wei N, Cui H. Growth of porous ZnO single crystal hierarchical architectures with ultrahigh sensing performances to ethanol and acetone gases. *Ceramics International*. 2017;**43**(1):1121-1128. DOI: 10.1016/j.ceramint.2016.10.050
- [97] Wilson SA, Jourdain RPJ, Zhang Q, Dorey RA, Bowen CR, Willander M, Wahab QU, Al-hilli SM, Nur O, Quandt E, Johansson C, Pagounis E, Kohl M, Matovic J, Samel B, Van der Wijngaart W, Jager EWH, Carlsson D, Djinojic Z, Wegener M, Moldovan C, Iosub R, Abad E, Wendlandt M, Rusu C, Persson K. New materials for micro-scale sensors and actuators an engineering review. *Materials Science and Engineering*. 2007;**56**(1-6): 1-129. DOI: 10.1016/j.mser.2007.03.001
- [98] Divya T, Nikhila MP, Anju M, Arsha KTV, Akhila AK, Ravikiran YT, Renuka NK. Nanoceria based thin films as efficient humidity sensors. *Sensors and Actuators A*. 2017;**261**:85-93. DOI: 10.1016/j.sna.2017.05.008
- [99] Wang Y, Duan G, Zhu Y, Zhang H, Xu Z, Dai Z, Cai W. Room temperature H_2S gas sensing properties of In_2O_3 micro/nanostructured porous thin film and hydrolyzation-induced enhanced sensing mechanism. *Sensors and Actuators B*. 2016;**228**:74-84. DOI: 10.1016/j.snb.2016.01.002
- [100] Al-Salmana HS, Abdullaha MJ. Hydrogen gas sensing based on ZnO nanostructure prepared by RF-sputtering on quartz and PET substrates. *Sensors and Actuators B*. 2013;**181**:259-266. DOI: 10.1016/j.snb.2013.01.065

- [101] Wagner T, Waitz T, Roggenbuck J, Fröba M, Kohl CD, Tiemann M. Ordered mesoporous ZnO for gas sensing. *Thin Solid Films*. 2007;**515**(23):8360-8363. DOI: 10.1016/j.tsf.2007.03.021
- [102] Blanka TA, Eksperiandova LP, Belikov KN. Recent trends of ceramic humidity sensors development: A review. *Sensors and Actuators B*. 2016;**228**:416-442. DOI: 10.1016/j.snb.2016.01.015